

Giant overreflection of magnetohydrodynamic waves from inhomogeneous plasmas with nonuniform shear flows

SEULONG KIM¹ AND KIHONG KIM^{2,3}

¹*Research Institute for Basic Sciences, Ajou University, Suwon 16499, Korea*

²*Department of Physics, Ajou University, Suwon 16499, Korea*

³*School of Physics, Korea Institute for Advanced Study, Seoul 02455, Korea*

ABSTRACT

We study theoretically mode conversion and resonant overreflection of magnetohydrodynamic waves in an inhomogeneous plane-stratified plasma in the presence of a nonuniform shear flow, using precise numerical calculations of the reflection and transmission coefficients and the field distributions based on the invariant imbedding method. The cases where the flow velocity and the external magnetic field are directed perpendicularly to the inhomogeneity direction and both the flow velocity and the plasma density vary arbitrarily along it are considered. When there is a shear flow, the wave frequency is modulated locally by the Doppler shift and resonant amplification and overreflection occur where the modulated frequency is negative and its absolute value matches the local Alfvén or slow frequency. For many different types of the density and flow velocity profiles, we find that, especially when the parameters are such that the incident waves are totally reflected, there arises a giant overreflection where the reflectance is much larger than 10 in a fairly broad range of the incident angles, the frequency, and the plasma β and its maximum attains values larger than 10^5 . In a finite β plasma, both incident fast and slow magnetosonic waves are found to cause strong overreflection and there appear multiple positions exhibiting both Alfvén and slow resonances inside the plasma. We explain the mechanism of overreflection in terms of the formation of inhomogeneous and open cavities close to the resonances and the strong enhancement of the wave energy due to the occurrence of semi-bound states there. We give discussions of the observational consequences in magnetized terrestrial and solar plasmas.

Keywords: Magnetohydrodynamics (1964) — Space plasmas (1544) — Plasma astrophysics (1261) — Alfvén waves (23) — Planetary magnetospheres (997) — Solar corona (1483)

1. INTRODUCTION

Understanding the processes of electromagnetic wave propagation in inhomogeneous complex plasmas plays a central role in various areas of plasma physics and astrophysics (Keiling et al. 2016; Walker 2005; Roberts 2019). In this paper, we investigate theoretically the propagation of magnetohydrodynamic (MHD) waves in the presence of a *nonuniform* shear flow of plasma. Mode conversion and the associated resonant absorption of electromagnetic waves in inhomogeneous plasmas have been studied extensively for many decades (Swanson 1998; Forslund et al. 1975; Mjølhus 1990; Hinkel-Lipsker et al. 1992; Kim & Lee 2005, 2006; Kim et al. 2007; DeDougall

& Hood 2007; Lee et al. 2008; Yu & Nakariakov 2020). In the low-frequency regime where magnetohydrodynamics is applicable, there can exist three kinds of wave modes in uniform plasmas, namely, shear Alfvén waves and fast and slow magnetosonic waves, among which slow magnetosonic waves are excited only in finite temperature plasmas. When fast or slow magnetosonic waves with frequencies in the Alfvén or slow continuum are incident onto inhomogeneous stratified MHD plasmas, the wave frequency can match that of the local Alfvén or slow (or cusp) oscillations at some resonance positions, which causes the localized Alfvén or slow resonance and the resonant absorption of the wave energy. This phenomenon, especially the Alfvén resonance that has often been called the field line resonance (FLR), has been suggested to be very important for the heating of a plasma and the transport of the wave energy (Chen & Hasegawa

1974a; Southwood 1974; Leonovich & Kozlov 2013; Lee et al. 2002; Lysak 2022). There have been proposals that the FLR is relevant for the excitation of ultra-low-frequency (ULF) magnetic pulsations in the terrestrial magnetosphere (Chen & Hasegawa 1974b) and solar coronal heating (Nakariakov et al. 2016; Nakariakov & Kolotkov 2020; Van Doorselaere et al. 2020).

In the theories of ULF pulsations based on the FLR, there has been emphasis on two important features, which are the cavity- and waveguide-like effects of the inhomogeneous boundary region between the magnetosheath and the magnetosphere and the shear flow due to the abrupt change of the flow velocity from the magnetosheath into the magnetosphere (Walker 1998, 2000; Mazur & Chuiko 2013). In many theoretical and observational studies, it has been argued that the excitation and properties of Pc 3–5 pulsations can be explained from such considerations.

When there is a shear flow of plasma, the FLR can occur in a significantly different manner. The effective frequency of MHD waves is modulated by the Doppler effect due to plasma flow and a *negative* effective frequency can arise when the flow speed is sufficiently high. In such a case, waves gain energy from the shear flow and the phenomenon of overreflection with the reflectance larger than 1 occurs (McKenzie 1969; Cairns 1979; Mann et al. 1999). In plane-stratified plasmas, resonant amplification and overreflection occur at the planes where the modulated frequency is negative and its absolute value is equal to the local Alfvén or slow frequency.

The overreflection phenomena are expected to take place generally in magnetized plasmas with structured inhomogeneity and strong flow shear. The examples in space physics and solar physics include magnetopause and magnetotail regions in planetary magnetospheres and coronal loops, plumes, and magnetic reconnection regions in the solar atmosphere. Csík et al. (1998, 2000) have studied theoretically the effects of a stationary mass flow on resonant absorption and overreflection in low β solar plasmas. They have considered a model where the Alfvén velocity varies linearly while the shear flow velocity has a step-function profile and calculated the absorption coefficient as a function of flow speed and frequency, when waves are incident from a high density region with no flow to a low density region with a uniform flow. The incident angle has been fixed to a single value and only the configurations where the incident wave is totally reflected have been considered. Their results have demonstrated that for both fast and slow magnetosonic waves, overreflection as well as resonant absorption can be obtained depending on the parameters. The numerically obtained maximum values of

the absorption coefficient and the reflectance have been found to be about 0.7 and 3.5 respectively. The results have been compared with the parameters for the solar atmosphere.

In this paper, we generalize the study of Csík et al. (1998, 2000) to the case where both the flow velocity and the plasma density vary arbitrarily along the inhomogeneity direction. Based on the invariant imbedding method (IIM) (Bellman 1976; Klyatskin 2005; Golberg 1975; Kim & Lee 2005, 2006; Kim & Kim 2016a), we develop a numerical method to solve the MHD wave equation and calculate the reflection and transmission coefficients and the field distributions in a numerically precise manner for an *entire range of the incident angles*. For many different types of the density and flow velocity profiles, we find that, especially when the parameters are such that the incident waves are totally reflected, giant overreflection where the reflectance is much larger than 10 in a fairly broad range of the incident angles, the frequency, and the plasma β occurs and its maximum attains values larger than 10^5 . We find that in a finite β plasma, both fast and slow magnetosonic waves cause strong overreflection and there appear multiple positions exhibiting both Alfvén and slow resonances inside the plasma. Our results also include the overreflection phenomena occurring when the incident wave propagates in the transmitted region with negative energy. We explain the mechanism of giant overreflection in terms of the formation of inhomogeneous and open cavities close to the resonances and the strong enhancement of the wave energy due to the formation of semi-bound states there. We also give some discussions on the possible consequences of our theory in magnetized terrestrial and solar plasmas. Giant overreflection with a similar mechanism has been previously studied in the context of amplification of circularly-polarized electromagnetic waves in chiral optical media with gain (Kim & Kim 2016b).

It is worth mentioning the merits of the IIM used in the present work. Using this method, it is possible to solve the MHD wave equation in the general cases where the external magnetic field as well as the plasma density and the flow velocity varies arbitrarily along the inhomogeneity direction. Although the wave equation becomes *singular* in the presence of resonances, we are able to solve it in a numerically exact manner without using any approximation such as the WKB approximation. We propose that the IIM can be a very useful tool in the study of wave propagation problems in a variety of astrophysical plasmas.

The rest of this paper is organized as follows. In Section 2, we develop the basic MHD theory and derive

the wave equations used in this study. In Section 3, we discuss the IIM and present the invariant imbedding equations. A simplified version of the theory in the case of cold plasmas is given in Section 4. In Section 5, we present extensive numerical results obtained by using the IIM for various configurations of the plasma density and the flow velocity. In Section 6, we provide an explanation of the mechanism of giant overreflection. Some discussions on the observational consequences of the theory are given in Section 7. Finally, we conclude the paper in Section 8.

2. WAVE EQUATION

We start with the standard set of ideal MHD equations

$$\begin{aligned} \frac{\partial \rho}{\partial t} + \nabla \cdot (\rho \mathbf{v}) &= 0, \\ \frac{\partial \mathbf{v}}{\partial t} + (\mathbf{v} \cdot \nabla) \mathbf{v} &= -\frac{\nabla p}{\rho} + \frac{1}{\mu_0 \rho} (\nabla \times \mathbf{B}) \times \mathbf{B}, \\ \frac{\partial p}{\partial t} + (\mathbf{v} \cdot \nabla) p &= \frac{\gamma p}{\rho} \left[\frac{\partial \rho}{\partial t} + (\mathbf{v} \cdot \nabla) \rho \right], \\ \frac{\partial \mathbf{B}}{\partial t} &= \nabla \times (\mathbf{v} \times \mathbf{B}), \\ \nabla \cdot \mathbf{B} &= 0, \end{aligned} \quad (1)$$

where \mathbf{v} , \mathbf{B} , ρ , and p are the fluid velocity, the magnetic field, the mass density, and the pressure respectively. γ is the ratio of the specific heats and μ_0 is the vacuum magnetic permeability. We have ignored the gravitational field here. We consider the situation where a nonuniform plasma layer is placed in the region $0 \leq z \leq L$ and is surrounded by two semi-infinite uniform plasma layers. The nonuniform plasma is stratified and its medium parameters are assumed to depend only on the coordinate z . Plane waves are assumed to be incident from the region $z > L$ and transmitted to the region $z < 0$.

We linearize the MHD equations by substituting $\rho = \rho_0 + \rho_1$, $\mathbf{v} = \mathbf{v}_0 + \mathbf{v}_1$, $p = p_0 + p_1$, and $\mathbf{B} = \mathbf{B}_0 + \mathbf{B}_1$, where ρ_0 , \mathbf{v}_0 , p_0 , and \mathbf{B}_0 are the zeroth-order background quantities. Inside the nonuniform layer, these quantities generally depend on z and are time-independent. Then the zeroth-order equation of continuity takes the form

$$\frac{d}{dz} (\rho_0 v_{0z}) = 0, \quad (2)$$

where v_{0z} is the z component of \mathbf{v}_0 . Barring the improbable situation where $\rho_0(z)$ is strictly proportional to $[v_{0z}(z)]^{-1}$, this equation can be satisfied only when $v_{0z} = 0$. That is, there is no equilibrium flow in the direction of inhomogeneity. Furthermore, when $v_{0z} = 0$,

the zeroth-order forms of Faraday's equation and $\nabla \cdot \mathbf{B} = 0$ lead to

$$\frac{d}{dz} (v_{0x} B_{0z}) = \frac{d}{dz} (v_{0y} B_{0z}) = \frac{dB_{0z}}{dz} = 0. \quad (3)$$

Since the flow velocity \mathbf{v}_0 is not uniform in the whole space, we obtain the condition $B_{0z} = 0$. We note that if \mathbf{v}_0 were uniform in the whole space, we could have chosen a reference frame moving with the same velocity and removed \mathbf{v}_0 from the equations. From these considerations, we assume, with no loss of generality, that $\mathbf{B}_0 = B_0(z) \hat{\mathbf{x}}$ and $\mathbf{v}_0 = U_x(z) \hat{\mathbf{x}} + U_y(z) \hat{\mathbf{y}}$. The z dependence of U_x and U_y implies that there is a nonuniform shear flow in the direction perpendicular to that of inhomogeneity.

From the zeroth-order momentum equation, we obtain

$$\frac{d}{dz} \left(p_0 + \frac{B_0^2}{2\mu_0} \right) = 0, \quad (4)$$

where the expression $p_0 + B_0^2/(2\mu_0)$ is the equilibrium total pressure which is a constant. If the external magnetic field is uniform in the whole space, the equilibrium pressure p_0 is also uniform.

To the first order in the perturbed quantities, we get

$$\begin{aligned} \frac{\partial \rho_1}{\partial t} + \nabla \cdot (\rho_0 \mathbf{v}_1) + (\mathbf{v}_0 \cdot \nabla) \rho_1 &= 0, \\ \rho_0 \frac{\partial \mathbf{v}_1}{\partial t} + \rho_0 (\mathbf{v}_0 \cdot \nabla) \mathbf{v}_1 + \rho_0 (\mathbf{v}_1 \cdot \nabla) \mathbf{v}_0 &= -\nabla p_1 \\ &+ \frac{1}{\mu_0} (\nabla \times \mathbf{B}_0) \times \mathbf{B}_1 + \frac{1}{\mu_0} (\nabla \times \mathbf{B}_1) \times \mathbf{B}_0, \\ \frac{\partial p_1}{\partial t} + (\mathbf{v}_1 \cdot \nabla) p_0 + (\mathbf{v}_0 \cdot \nabla) p_1 &= v_s^2 \left[\frac{\partial \rho_1}{\partial t} + (\mathbf{v}_1 \cdot \nabla) \rho_0 + (\mathbf{v}_0 \cdot \nabla) \rho_1 \right], \\ \frac{\partial \mathbf{B}_1}{\partial t} = \nabla \times (\mathbf{v}_1 \times \mathbf{B}_0) + \nabla \times (\mathbf{v}_0 \times \mathbf{B}_1), & \\ \nabla \cdot \mathbf{B}_1 = 0, & \end{aligned} \quad (5)$$

where the speed of sound v_s is defined by

$$v_s = \sqrt{\frac{\gamma p_0}{\rho_0}}. \quad (6)$$

In the uniform regions, we can Fourier analyze Eq. (5) by making the substitutions $\nabla \rightarrow i\mathbf{k}$ and $\partial/\partial t \rightarrow -i\omega$. We assume that the wave vector is in an arbitrary direction and write its components as

$$k_x = k \sin \theta \cos \phi, \quad k_y = k \sin \theta \sin \phi, \quad k_z = k \cos \theta, \quad (7)$$

where θ ($0 \leq \theta < \pi/2$) is defined as the angle between \mathbf{k} and the *negative* z direction and k_z is the *negative* z component of the wave vector. The angle ϕ is the azimuthal

angle of the wave vector ($0 \leq \phi < 2\pi$). Following the standard procedure for deriving the dispersion relations for MHD waves, we obtain

$$\frac{\Omega^2}{k^2} = \frac{1}{2} (v_A^2 + v_s^2) + \frac{1}{2} \left[(v_A^2 + v_s^2)^2 - 4v_A^2 v_s^2 \sin^2 \theta \cos^2 \phi \right]^{1/2}, \quad (8)$$

$$\frac{\Omega^2}{k^2} = \frac{1}{2} (v_A^2 + v_s^2) - \frac{1}{2} \left[(v_A^2 + v_s^2)^2 - 4v_A^2 v_s^2 \sin^2 \theta \cos^2 \phi \right]^{1/2}, \quad (9)$$

$$\frac{\Omega^2}{k^2} = v_A^2 \sin^2 \theta \cos^2 \phi, \quad (10)$$

where v_A is the Alfvén velocity defined by

$$v_A = \frac{B_0}{\sqrt{\mu_0 \rho_0}} \quad (11)$$

and Ω is the wave frequency shifted by the Doppler effect in the presence of a mass flow and is given by

$$\Omega = \omega - U_x k_x - U_y k_y. \quad (12)$$

We note that the quantity $\sin \theta \cos \phi$ is equal to the cosine of the angle between \mathbf{k} and \mathbf{B}_0 . The first two dispersion relations, Eqs. (8) and (9), correspond to the fast and slow magnetosonic modes respectively, while the third dispersion relation, Eq. (10), corresponds to the transverse Alfvén mode. These dispersion relations differ from the usual ones only in that the frequency ω is replaced by Ω .

In the nonuniform region where the medium parameters depend on z , we substitute

$$\begin{aligned} \rho_1 &= \tilde{\rho}(z) e^{i(k_x x + k_y y - \omega t)}, \\ \mathbf{v}_1 &= \tilde{\mathbf{v}}(z) e^{i(k_x x + k_y y - \omega t)}, \\ p_1 &= \tilde{p}(z) e^{i(k_x x + k_y y - \omega t)}, \\ \mathbf{B}_1 &= \tilde{\mathbf{B}}(z) e^{i(k_x x + k_y y - \omega t)} \end{aligned} \quad (13)$$

into Eq. (5) and derive the ordinary differential equations satisfied by the variables $\tilde{\rho}$, $\tilde{\mathbf{v}}$, \tilde{p} , and $\tilde{\mathbf{B}}$. It turns out that we can combine these equations into two first-order differential equations of the form

$$\frac{dP}{dz} = A \xi_z, \quad \frac{d\xi_z}{dz} = -\frac{C}{D} P, \quad (14)$$

where

$$\begin{aligned} A &= \rho_0 (\Omega^2 - \omega_A^2), \\ C &= (\Omega^2 - \omega_A^2) (\Omega^2 - \omega_s^2) - \Omega^2 v_A^2 k_y^2, \\ D &= \rho_0 (v_A^2 + v_s^2) (\Omega^2 - \omega_A^2) (\Omega^2 - \omega_c^2). \end{aligned} \quad (15)$$

The parameters ω_A , ω_s , and ω_c are defined by

$$\begin{aligned} \omega_A^2 &= k_x^2 v_A^2, \quad \omega_s^2 = (k_x^2 + k_y^2) v_s^2, \\ \omega_c^2 &= k_x^2 v_c^2, \end{aligned} \quad (16)$$

where the cusp velocity v_c is given by

$$v_c = \frac{v_A v_s}{\sqrt{v_A^2 + v_s^2}}. \quad (17)$$

Note that the cusp frequency ω_c is unrelated to the cyclotron frequency. The variables P and ξ_z are defined by

$$P = \tilde{p} + \frac{B_0}{\mu_0} \tilde{B}_x, \quad \xi_z = i \frac{\tilde{v}_z}{\Omega}. \quad (18)$$

P corresponds to the first-order perturbation of the total pressure $p + B^2/(2\mu_0)$ and ξ_z is the z component of the Lagrangian displacement vector. From Eq. (14), we can derive the second-order differential equations satisfied by P and ξ_z :

$$\frac{d}{dz} \left(\frac{1}{A} \frac{dP}{dz} \right) + \frac{C}{D} P = 0, \quad (19)$$

$$\frac{d}{dz} \left(\frac{D}{C} \frac{d\xi_z}{dz} \right) + A \xi_z = 0. \quad (20)$$

We can solve either of these equations to obtain $P(z)$ or $\xi_z(z)$, and then calculate all other variables $\tilde{\rho}$, $\tilde{\mathbf{v}}$, \tilde{p} , $\tilde{\mathbf{B}}$, and the perturbed electric field $\tilde{\mathbf{E}}$ using simple relationships among the variables. For instance, we can express \tilde{E}_y in terms of ξ_z by

$$\tilde{E}_y = i (\omega - U_y k_y) B_0 \xi_z. \quad (21)$$

In the case where the flow velocity is parallel to \mathbf{B}_0 (that is, when $U_y = 0$), equations equivalent to Eq. (14) were first derived in Čadež et al. (1997).

From the form of the wave equation, Eq. (19), we notice that it becomes *singular* at the positions $z = z_A$ and $z = z_c$ satisfying

$$\Omega(z_A) = \pm \omega_A(z_A), \quad \Omega(z_c) = \pm \omega_c(z_c). \quad (22)$$

The resonances at z_A and z_c are called the Alfvén resonance and the slow (or cusp) resonance respectively. We observe that the shifted frequency Ω can be either positive or negative. When it is positive, we have

$$\begin{aligned} \omega &= U_x k_x + U_y k_y + \omega_A, \\ \omega &= U_x k_x + U_y k_y + \omega_c, \end{aligned} \quad (23)$$

which implies that the energy of the incident wave is converted to that of the local Alfvén mode or slow MHD

mode and the resonant wave absorption occurs. In contrast, when Ω is negative, we have

$$\begin{aligned} U_x k_x + U_y k_y &= \omega + \omega_A, \\ U_x k_x + U_y k_y &= \omega + \omega_c, \end{aligned} \quad (24)$$

which implies that the flow supplies energy to the wave and the resonant amplification occurs. In this case, the reflectance becomes greater than one, resulting in the phenomenon of *overreflection*.

The parameter C in Eq. (15) can be factorized as

$$C = (\Omega^2 - \omega_I^2) (\Omega^2 - \omega_{II}^2), \quad (25)$$

where

$$\begin{aligned} \omega_I^2 &= \frac{1}{2} (v_A^2 + v_s^2) (k_x^2 + k_y^2) \\ &\times \left\{ 1 - \left[1 - \frac{4\omega_c^2}{(v_A^2 + v_s^2) (k_x^2 + k_y^2)} \right]^{1/2} \right\}, \\ \omega_{II}^2 &= \frac{1}{2} (v_A^2 + v_s^2) (k_x^2 + k_y^2) \\ &\times \left\{ 1 + \left[1 - \frac{4\omega_c^2}{(v_A^2 + v_s^2) (k_x^2 + k_y^2)} \right]^{1/2} \right\}. \end{aligned} \quad (26)$$

In the uniform regions, we can derive

$$k_z^2 = \frac{AC}{D} = \frac{(\Omega^2 - \omega_I^2) (\Omega^2 - \omega_{II}^2)}{(v_A^2 + v_s^2) (\Omega^2 - \omega_c^2)} \quad (27)$$

from Eq. (19) or (20). Using the condition $k_z = 0$ in Eqs. (8) and (9), we can show that $\Omega^2 = \omega_I^2$ and $\Omega^2 = \omega_{II}^2$ correspond to the *cutoff* conditions for the slow and fast magnetosonic waves in uniform media respectively. It is straightforward to prove the inequalities

$$\omega_c \leq \omega_I \leq \omega_A \leq \omega_{II}. \quad (28)$$

When $\Omega^2 > \omega_{II}^2$, fast magnetosonic waves can propagate in the medium, while, when $\omega_c^2 < \Omega^2 < \omega_I^2$, slow magnetosonic waves can. Waves become evanescent in the frequency region where $\Omega^2 < \omega_c^2$ or $\omega_I^2 < \Omega^2 < \omega_{II}^2$, which includes $\Omega^2 = \omega_A^2$.

By taking the derivative of Eq. (27) with respect to Ω , we can derive the relationship between the z component of the phase velocity, V_{pz} ($= \Omega/k_z$), and that of the group velocity, V_{gz} ($= \partial\Omega/\partial k_z$), for magnetosonic waves in uniform media of the form

$$V_{pz} V_{gz} = \frac{(v_A^2 + v_s^2) (\Omega^2 - \omega_c^2)^2}{(\Omega^2 - \omega_c^2)^2 - (\omega_I^2 - \omega_c^2) (\omega_{II}^2 - \omega_c^2)}. \quad (29)$$

We easily verify that for fast magnetosonic waves with $\Omega^2 > \omega_{II}^2$, this expression is positive and therefore V_{pz} and V_{gz} have the same signs. On the other hand, for slow magnetosonic waves with $\omega_c^2 < \Omega^2 < \omega_I^2$, $V_{pz} V_{gz}$ is negative and V_{pz} and V_{gz} have the opposite signs.

3. INVARIANT IMBEDDING METHOD

Using the IIM, we can accurately and efficiently solve the wave equation, Eq. (19), in the cases where the plasma density ρ_0 , the flow velocity components U_x and U_y , and the external magnetic field B_0 depend on z in an *arbitrary* manner in the region $0 \leq z \leq L$. We point out that, in general, the quantities v_A , v_s , v_c , ω_A , ω_s , ω_c , Ω , A , C , and D also depend on z . Alternatively, we may choose to solve Eq. (20). We have verified explicitly that the final numerical results are the same regardless of the choice of wave equation.

In the IIM, we first calculate the reflection and transmission coefficients r and t defined by the wave functions in the incident and transmitted regions:

$$P(z, L) = \begin{cases} e^{ik_{z1}(L-z)} + r(L)e^{ik_{z1}(z-L)}, & z > L \\ t(L)e^{-ik_{z2}z}, & z < 0 \end{cases}, \quad (30)$$

where k_{z1} and k_{z2} are the negative z components of the wave vector in the incident and transmitted regions respectively and r and t are regarded as functions of L . We assume that the waves are not evanescent in the incident region and therefore k_{z1} is a real number. Since V_{pz} and V_{gz} have the same (opposite) signs for fast (slow) waves, we have to choose k_{z1} to be positive (negative) for fast (slow) waves. We obtain

$$k_{z1} = \begin{cases} \sqrt{\frac{A_1 C_1}{D_1}} & \text{for fast waves} \\ -\sqrt{\frac{A_1 C_1}{D_1}} & \text{for slow waves} \end{cases}, \quad (31)$$

where A_1 , C_1 , and D_1 are the values of A , C , and D in the incident region and $A_1 C_1 / D_1$ is assumed to be positive. In the transmitted region where $z < 0$, the waves can be either propagative or evanescent depending on the sign of $A_2 C_2 / D_2$, where A_2 , C_2 , and D_2 are the values of A , C , and D in the transmitted region. We define k_{z2} by

$$k_{z2} = \begin{cases} \sqrt{\frac{A_2 C_2}{D_2}} & \text{for fast waves, } \frac{A_2 C_2}{D_2} > 0, \Omega_2 > 0 \\ -\sqrt{\frac{A_2 C_2}{D_2}} & \text{for fast waves, } \frac{A_2 C_2}{D_2} > 0, \Omega_2 < 0 \\ -\sqrt{\frac{A_2 C_2}{D_2}} & \text{for slow waves, } \frac{A_2 C_2}{D_2} > 0, \Omega_2 > 0 \\ \sqrt{\frac{A_2 C_2}{D_2}} & \text{for slow waves, } \frac{A_2 C_2}{D_2} > 0, \Omega_2 < 0 \\ i\sqrt{\left| \frac{A_2 C_2}{D_2} \right|} & \text{for } \frac{A_2 C_2}{D_2} \leq 0 \end{cases}, \quad (32)$$

where Ω_2 is the value of Ω in the transmitted region. The choices of sign for the propagative cases are made to make sure that the group velocity in the region $z < 0$ is always in the negative z direction.

Following the procedure given in Kim & Kim (2016a), we derive the invariant imbedding equations satisfied by

r and t :

$$\begin{aligned} \frac{dr}{dl} &= 2ik_{z1} \frac{A}{A_1} r + \frac{i}{2k_{z1}} \left(\frac{CA_1}{D} - \frac{A}{A_1} k_{z1}^2 \right) (1+r)^2, \\ \frac{dt}{dl} &= ik_{z1} \frac{A}{A_1} t + \frac{i}{2k_{z1}} \left(\frac{CA_1}{D} - \frac{A}{A_1} k_{z1}^2 \right) (1+r)t. \end{aligned} \quad (33)$$

We notice that the parameter D appears in the denominator and the singularity at the resonances corresponding to $D = 0$ is clearly exhibited in the invariant imbedding equations. The resonance conditions for the incident fast and slow waves can be expressed more explicitly as

$$\begin{aligned} f_1(z) &= F - \frac{U_x(z)}{v_{A1}} \sin \theta \cos \phi - \frac{U_y(z)}{v_{A1}} \sin \theta \sin \phi - \sqrt{\frac{\rho_{01}}{\rho_0(z)}} |\sin \theta \cos \phi| = 0, \\ f_2(z) &= F - \frac{U_x(z)}{v_{A1}} \sin \theta \cos \phi - \frac{U_y(z)}{v_{A1}} \sin \theta \sin \phi + \sqrt{\frac{\rho_{01}}{\rho_0(z)}} |\sin \theta \cos \phi| = 0, \\ f_3(z) &= F - \frac{U_x(z)}{v_{A1}} \sin \theta \cos \phi - \frac{U_y(z)}{v_{A1}} \sin \theta \sin \phi - \sqrt{\frac{\gamma\beta(z)}{2 + \gamma\beta(z)}} \sqrt{\frac{\rho_{01}}{\rho_0(z)}} |\sin \theta \cos \phi| = 0, \\ f_4(z) &= F - \frac{U_x(z)}{v_{A1}} \sin \theta \cos \phi - \frac{U_y(z)}{v_{A1}} \sin \theta \sin \phi + \sqrt{\frac{\gamma\beta(z)}{2 + \gamma\beta(z)}} \sqrt{\frac{\rho_{01}}{\rho_0(z)}} |\sin \theta \cos \phi| = 0, \end{aligned} \quad (34)$$

where

$$F = \begin{cases} \frac{1}{2} \sqrt{2 + \gamma\beta_1 + \sqrt{(2 + \gamma\beta_1)^2 - 8\gamma\beta_1 \sin \theta \cos \phi}} & \text{for fast-wave incidence} \\ \frac{1}{2} \sqrt{2 + \gamma\beta_1 - \sqrt{(2 + \gamma\beta_1)^2 - 8\gamma\beta_1 \sin \theta \cos \phi}} & \text{for slow-wave incidence} \end{cases}. \quad (35)$$

The plasma β parameter is defined by

$$\beta(z) = \frac{2\mu_0 p_0(z)}{[B_0(z)]^2} \quad (36)$$

and is generally a function of z . The parameters ρ_{01} , v_{A1} , and β_1 are the mass density, the Alfvén velocity, and the plasma β in the incident region respectively. The condition $f_1 = 0$ ($f_2 = 0$) corresponds to the resonant absorption (amplification) due to the Alfvén resonance with $\Omega = \omega_A$ ($\Omega = -\omega_A$), whereas $f_3 = 0$ ($f_4 = 0$) does to the resonant absorption (amplification) due to the slow resonance with $\Omega = \omega_c$ ($\Omega = -\omega_c$).

We calculate $r(L)$ and $t(L)$ by integrating Eq. (33) numerically from $l = 0$ to $l = L$ using the initial conditions

$$r(0) = \frac{k_{z1}A_2 - k_{z2}A_1}{k_{z1}A_2 + k_{z2}A_1}, \quad t(0) = \frac{2k_{z1}A_2}{k_{z1}A_2 + k_{z2}A_1}. \quad (37)$$

The reflectance R and the transmittance T are obtained using

$$R = |r|^2, \quad T = \begin{cases} \frac{k_{z2}A_1}{k_{z1}A_2} |t|^2 & \text{if } \frac{A_2 C_2}{D_2} > 0 \\ 0 & \text{if } \frac{A_2 C_2}{D_2} \leq 0 \end{cases}. \quad (38)$$

As we have mentioned already, we can assume that the flow velocity is zero in the incident region. Then Ω ($= \omega$) is positive in that region. If Ω_2 is also positive in the propagative case, k_{zi} ($i = 1, 2$) is positive for fast waves and negative for slow waves, but at the same time A_i has the same sign as k_{zi} due to the inequalities in Eq. (28). Therefore the transmittance T is positive. In contrast, when Ω_2 is negative, k_{z2} and A_2 have the opposite signs for both fast and slow waves and T becomes negative. This latter case corresponding to the negative transmittance can be considered as an example of a wave with a negative energy and is caused by the Doppler shift of Ω to a negative value due to a fast flow of the plasma (Ostrovskii et al. 1986; Joarder et al. 1997). In such a case, the signs of the frequencies of the incident and transmitted waves are opposite to each other and overreflection with $R > 1$ can occur due to the energy exchange between positive and negative energy waves. However, the giant overreflection phenomenon which is the primary focus of this paper is caused primarily not by negative energy waves, but by the mode conversion between the

incident wave and resonant local oscillations when the transmitted wave is evanescent and the transmittance is zero.

In realistic plasmas, there always exists some amount of dissipation due to collisions, the effects of which can be incorporated into the formalism by replacing ω with $\omega + i\nu$, where ν (> 0) is the collision frequency. The inclusion of the imaginary part of the frequency removes the singularities at the resonances and allows us to solve Eq. (33) numerically for any spatial configurations of ρ_0 , U_x , U_y , and B_0 . In general, ν may depend on various parameters including frequency and also on the spatial coordinates. Since the resonant absorption or amplification due to mode conversion occurs even in the limit where $\nu \rightarrow 0$, we will choose a sufficiently small value of ν in most of our numerical calculations. In such cases, all the results will be independent of the numerical value of ν used in the calculations.

The IIM can also be used in calculating the wave function $P = P(z; L)$, which we consider as a function of both z and L , inside the inhomogeneous region. The equation satisfied by $P(z; L)$ is very similar to that for t and takes the form

$$\frac{\partial}{\partial l} P(z; l) = ik_{z1} \frac{A(l)}{A_1} P(z; l) + \frac{i}{2k_{z1}} \left[\frac{C(l)A_1}{D(l)} - \frac{A(l)}{A_1} k_{z1}^2 \right] [1 + r(l)] P(z; l). \quad (39)$$

This equation is integrated from $l = z$ to $l = L$ using the initial condition $P(z; z) = 1 + r(z)$ to obtain $P(z; L)$.

4. COLD MHD LIMIT

In a cold plasma where the temperature is sufficiently low, we can set $p_0 = v_s = v_c = 0$ and ignore the pressure field \tilde{p} . Then the slow magnetosonic mode and the slow resonance are absent and only the fast magnetosonic and transverse Alfvén modes and the Alfvén resonance remain to occur. We restrict our interest to the special case where B_0 is uniform in the whole space and $U_y = 0$ while $U_x \neq 0$. We also assume that U_x is zero in the incident region. Then we can rewrite the wave equation, Eq. (19), in a simplified form as

$$\frac{d}{dz} \left(\frac{1}{\epsilon} \frac{d\tilde{B}_x}{dz} \right) + \left(k_0^2 - \frac{k_y^2}{\epsilon} \right) \tilde{B}_x = 0, \quad (40)$$

where

$$\epsilon = \frac{\rho_0(z)}{\rho_{01}} \left[1 - \frac{U_x(z)}{v_{A1}} \sin \theta \cos \phi \right]^2 - \sin^2 \theta \cos^2 \phi, \quad (41)$$

$$k_0 = \frac{\omega}{v_{A1}}, \quad k_y = k_0 \sin \theta \sin \phi.$$

The Alfvén resonance occurs at the positions satisfying $\epsilon = 0$. The resonance condition can be expressed as

$$f_{c1} = 1 - \frac{U_x(z)}{v_{A1}} \sin \theta \cos \phi - \sqrt{\frac{\rho_{01}}{\rho_0(z)}} |\sin \theta \cos \phi| = 0,$$

$$f_{c2} = 1 - \frac{U_x(z)}{v_{A1}} \sin \theta \cos \phi + \sqrt{\frac{\rho_{01}}{\rho_0(z)}} |\sin \theta \cos \phi| = 0. \quad (42)$$

The singularity at the Alfvén resonance can be taken care of by replacing ϵ in Eq. (41) with

$$\epsilon = \frac{\rho_0(z)}{\rho_{01}} \left[1 + i\eta - \frac{U_x(z)}{v_{A1}} \sin \theta \cos \phi \right]^2 - \sin^2 \theta \cos^2 \phi, \quad (43)$$

$$\eta = \frac{\nu}{\omega},$$

in the inhomogeneous region. The damping parameter η is chosen to be a sufficiently small positive number. Even though η is always positive, the imaginary part of ϵ becomes negative if $(U_x/v_{A1}) \sin \theta \cos \phi > 1$, which leads to wave amplification and overreflection.

The invariant imbedding equations for r and t take the simplified forms

$$\frac{dr}{dl} = 2ik_{z1} \frac{\epsilon}{\epsilon_1} r + \frac{i}{2k_{z1}} \left(k_0^2 \epsilon_1 - \frac{\epsilon_1}{\epsilon} k_y^2 - \frac{\epsilon}{\epsilon_1} k_{z1}^2 \right) (1+r)^2,$$

$$\frac{dt}{dl} = ik_{z1} \frac{\epsilon}{\epsilon_1} t + \frac{i}{2k_{z1}} \left(k_0^2 \epsilon_1 - \frac{\epsilon_1}{\epsilon} k_y^2 - \frac{\epsilon}{\epsilon_1} k_{z1}^2 \right) t(1+r), \quad (44)$$

where

$$\epsilon_1 = 1 - \sin^2 \theta \cos^2 \phi, \quad k_{z1} = k_0 \cos \theta. \quad (45)$$

The initial conditions are

$$r(0) = \frac{k_{z1}\epsilon_2 - k_{z2}\epsilon_1}{k_{z1}\epsilon_2 + k_{z2}\epsilon_1}, \quad t(0) = \frac{2k_{z1}\epsilon_2}{k_{z1}\epsilon_2 + k_{z2}\epsilon_1}, \quad (46)$$

where

$$\epsilon_2 = \frac{\rho_{02}}{\rho_{01}} \left[1 - \frac{U_{x2}}{v_{A1}} \sin \theta \cos \phi \right]^2 - \sin^2 \theta \cos^2 \phi, \quad (47)$$

$$k_{z2} = \begin{cases} \sqrt{k_0^2 \epsilon_2 - k_y^2} & \text{if } k_0^2 \epsilon_2 > k_y^2, \Omega_2 > 0 \\ -\sqrt{k_0^2 \epsilon_2 - k_y^2} & \text{if } k_0^2 \epsilon_2 > k_y^2, \Omega_2 < 0 \\ i\sqrt{k_y^2 - k_0^2 \epsilon_2} & \text{if } k_0^2 \epsilon_2 \leq k_y^2 \end{cases} \quad (48)$$

The quantities ρ_{02} and U_{x2} refer to the mass density and the flow velocity in the transmitted region

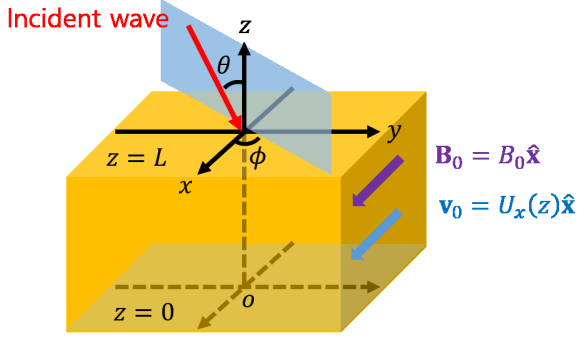


Figure 1. Schematic of the configuration considered in this paper.

respectively. The condition $\Omega_2 < 0$ is equivalent to $(U_{x2}/v_{A1}) \sin \theta \cos \phi > 1$. The transmittance T is obtained using

$$T = \begin{cases} \frac{k_{z2}\epsilon_1}{k_{z1}\epsilon_2} |t|^2 & \text{if } k_0^2 \epsilon_2 > k_y^2 \\ 0 & \text{if } k_0^2 \epsilon_2 \leq k_y^2 \end{cases} \quad (49)$$

When Ω_2 is negative in the propagative case, T becomes negative. The equation for the field amplitude \tilde{B}_x [= $\tilde{B}_x(z; l)$] takes the form

$$\frac{\partial}{\partial l} \tilde{B}_x(z; l) = ik_{z1} \frac{\epsilon(l)}{\epsilon_1} \tilde{B}_x(z; l) + \frac{i}{2k_{z1}} \left[k_0^2 \epsilon_1 - \frac{\epsilon_1}{\epsilon(l)} k_y^2 - \frac{\epsilon(l)}{\epsilon_1} k_{z1}^2 \right] [1 + r(l)] \tilde{B}_x(z; l), \quad (50)$$

which should be integrated from $l = z$ to $l = L$ using the initial condition $\tilde{B}_x(z; z) = 1 + r(z)$ to obtain $\tilde{B}_x(z; L)$.

5. NUMERICAL RESULTS

We restrict our attention to the case where the external magnetic field B_0 is uniform throughout the space. Then the equilibrium pressure p_0 and the plasma β are also uniform due to Eq. (4). From the ideal gas law, we obtain the relationship

$$\rho_0(z) T_0(z) = \text{constant} \quad (51)$$

between ρ_0 and the temperature T_0 . Furthermore, we consider only the case where the flow velocity is parallel or anti-parallel to \mathbf{B}_0 . Therefore U_y is zero, while U_x is nonzero. In the present situation, $\rho_0(z)$ and $U_x(z)$ can be specified independently by arbitrary functions. Instead of $\rho_0(z)$, we can equivalently choose to specify $v_A(z)$, $v_s(z)$, or $v_c(z)$. The ratio of the specific heats γ is chosen to be 5/3 which corresponds to an ideal monatomic gas. In Fig. 1, we show a simple schematic of the configuration considered in the present study.

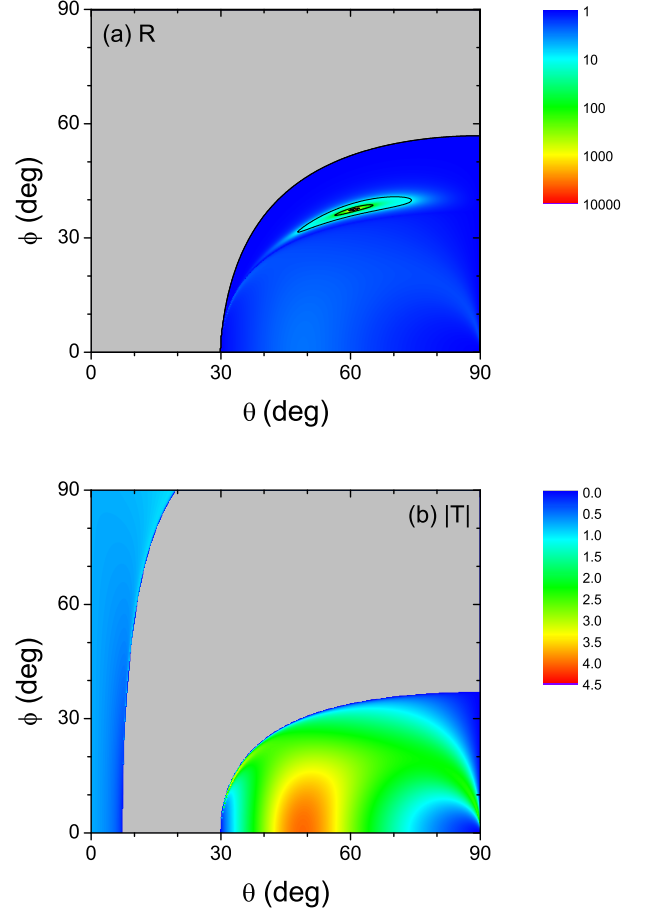


Figure 2. Contour plots of (a) the reflectance R and (b) the absolute value of the transmittance $|T|$ as functions of the incident angles θ and ϕ for the configuration given by Eq. (52), when the frequency ω of the incident fast wave is equal to $\omega_0 = v_{A1}/L$ and the plasma β is equal to zero. In the non-gray region of (a), R is larger than 1. In the gray region of (b), T is strictly zero.

We first consider the configuration where both U_x and v_A vary linearly in the region $0 \leq z \leq L$ such that

$$\frac{U_x(z)}{v_{A1}} = \begin{cases} 5, & \text{if } z < 0 \\ 5 \left(1 - \frac{z}{L}\right), & \text{if } 0 \leq z \leq L \\ 0, & \text{if } z > L \end{cases} \quad (52)$$

$$\frac{v_A(z)}{v_{A1}} = \begin{cases} 3, & \text{if } z < 0 \\ 3 - 2\frac{z}{L}, & \text{if } 0 \leq z \leq L \\ 1, & \text{if } z > L \end{cases}$$

In this configuration, since v_A is inversely proportional to $\sqrt{\rho_0}$, the wave incident from $z > L$ propagates from the region of higher density to that of lower density. We remind that we can always choose the flow velocity in the incident region to be zero by using the reference frame

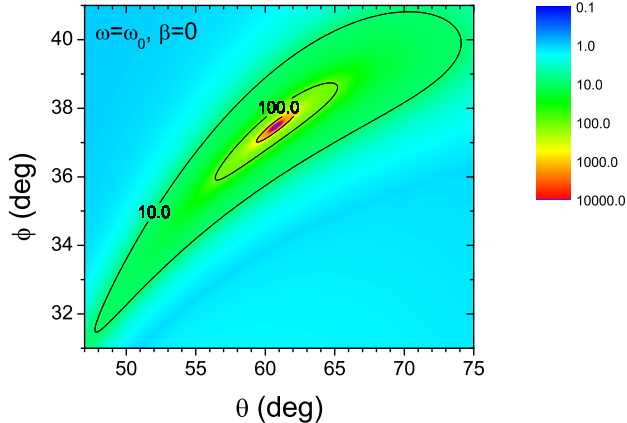


Figure 3. Expanded logarithmic contour plot of R as a function of θ and ϕ for the configuration given by Eq. (52), when $\omega = \omega_0$ and $\beta = 0$. The region of (θ, ϕ) such that $R > 10$ is explicitly displayed. In the narrow purple-colored region, R can be substantially larger than 10,000.

moving with that velocity. We consider the cold plasma case first and set the temperature T_0 and the plasma β to be zero. Then the slow magnetosonic wave is absent. We fix the frequency ω of the incident fast magnetosonic wave to ω_0 ($\equiv v_{A1}/L$) and the damping parameter η to 10^{-8} . We solve Eq. (44) numerically to obtain the reflectance R and the transmittance T as functions of the incident angles θ ($0 \leq \theta < \pi/2$) and ϕ ($0 \leq \phi < 2\pi$). We note that, due to symmetry, all physical quantities at $\phi = 2\pi - \phi_0$ are equal to those at $\phi = \phi_0$. According to Eq. (42), when $U_x(z)$ is positive, amplification is possible only when $\cos \phi$ is positive. Therefore we restrict the range of ϕ to $0 \leq \phi < \pi/2$. In Fig. 2, we show the logarithmic contour plot of R and the linear contour plot of the absolute value of T . In the non-gray region of Fig. 2(a), R is larger than 1. In the gray region of Fig. 2(b), T is strictly zero. We find that overreflection ($R > 1$) of the incident wave occurs in a substantial region of the (θ, ϕ) space. We also notice that *giant overreflection with $R \gtrsim 10$ occurs predominantly in the parameter region where the incident wave is totally reflected* and the transmittance is identically zero. In the region with $\theta \gtrsim 30^\circ$ and $\phi \lesssim 36^\circ$ in Fig. 2(b) where $|T|$ is substantially larger than 1, the transmittance is actually negative and overreflection arises due to negative energy waves in the transmitted region, not due to the mode conversion to local resonant MHD modes. However, the enhancement of the wave energy in this region is much smaller than in the region of giant overreflection shown explicitly in Fig. 3.

In Fig. 3, we show an expanded logarithmic contour plot of R mainly in the region where R is larger than 10.

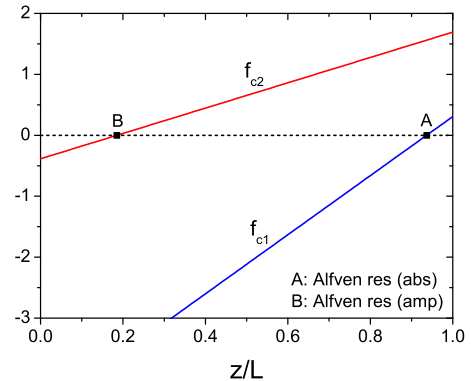


Figure 4. The functions f_{c1} and f_{c2} defined by Eq. (42) for the configuration given by Eq. (52) plotted versus z/L when $\theta = 60.8^\circ$ and $\phi = 37.5^\circ$, which corresponds to the maximum value of R in Fig. 3. The resonant absorption and amplification due to the Alfvén resonance occur at the positions A ($z/L \approx 0.937$) and B ($z/L \approx 0.185$) respectively.

Such a strong overreflection occurs in a fairly wide range of θ and in a narrower but readily measurable range of ϕ . We emphasize again that this region belongs to the gray region in Fig. 2(b) where the incident wave is totally reflected and the transmittance is zero. Inside the narrow purple-colored region, R can be substantially larger than 10,000. To the best of our knowledge, this type of giant overreflection has never been reported previously.

When a strong overreflection so that R is much greater than 10 occurs, there should be at least one resonance plane corresponding to the wave amplification with a negative effective damping parameter. In Fig. 4, we plot the functions f_{c1} and f_{c2} defined by Eq. (42) for the configuration given by Eq. (52) versus z/L when $\theta = 60.8^\circ$ and $\phi = 37.5^\circ$, which corresponds to the maximum of R in Fig. 3. The resonant absorption and amplification due to the Alfvén resonance occur at the positions A ($z/L \approx 0.937$) and B ($z/L \approx 0.185$) respectively. Strong amplification of the wave energy at B is responsible for the giant overreflection.

The phenomenon of strong overreflection persists in a wide range of incident wave frequency. In Fig. 5, we show the logarithmic contour plots of R at $\beta = 0$ when ω is equal to $0.5\omega_0$ and $1.5\omega_0$. The position and the shape of the region where R is greater than 10 in the (θ, ϕ) space are changed, but its size remains substantially large as the frequency varies.

In the present configuration, when $\omega = \omega_0$ and $\beta = 0$, the reflectance takes an extremely large maximum value at $\theta \approx 60.8^\circ$ and $\phi \approx 37.5^\circ$. The variations of R versus θ , ϕ , and ω close to the maximum are shown in Fig. 6. In Fig. 6(a), we observe that R is larger than 1 in the range

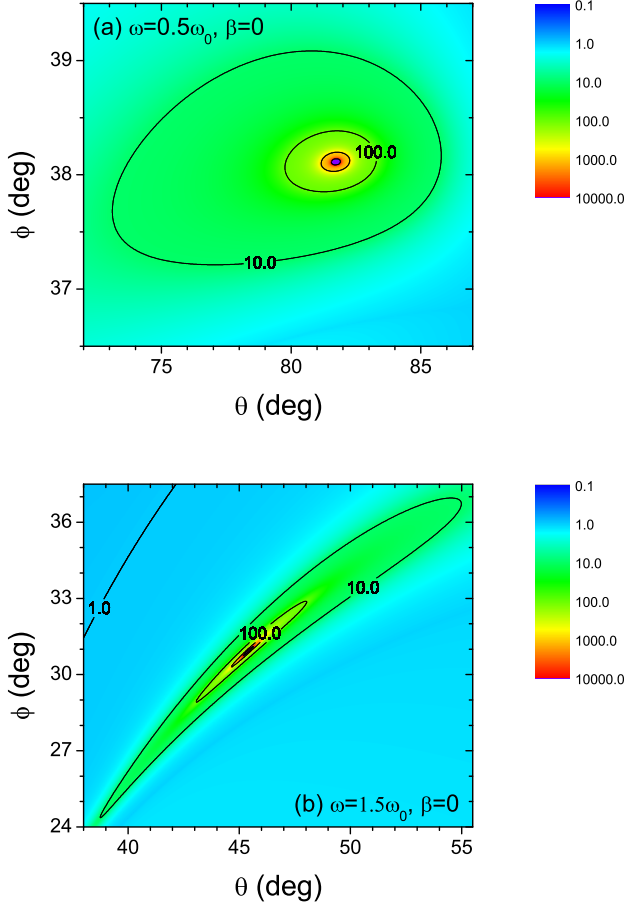


Figure 5. Logarithmic contour plots of R versus θ and ϕ for the configuration given by Eq. (52), when (a) $\omega = 0.5\omega_0$ and (b) $\omega = 1.5\omega_0$. The plasma β is zero.

$41.18^\circ < \theta < 90^\circ$, larger than 2 in $51.54^\circ < \theta < 80.92^\circ$, and larger than 10 in $56.6^\circ < \theta < 67.14^\circ$. In Fig. 6(b), we find that R is larger than 1 in $0^\circ < \phi < 51.92^\circ$, larger than 2 in $0^\circ < \phi < 33.9^\circ$ and in $34.12^\circ < \phi < 42.32^\circ$, and larger than 10 in $35.97^\circ < \phi < 39.15^\circ$. In this figure, the region where $\phi < 34^\circ$ corresponds to the region where overreflection occurs due to negative energy waves in the transmitted region. In Fig. 6(c), we find that R is larger than 1 in $0 < \omega/\omega_0 < 2.74$, larger than 2 in $0.43 < \omega/\omega_0 < 1.82$, and larger than 10 in $0.76 < \omega/\omega_0 < 1.28$. We notice that the maximum reflectance is well over 10^6 .

In the case of warm plasmas with finite β , we can solve Eq. (33) numerically to obtain R and T for both incident fast and slow waves. In Fig. 7, we show the logarithmic contour plots of R for fast waves of frequency $\omega = \omega_0$ when β is equal to 0.5 and 1. We find that the position of the region where R is larger than 10 in the (θ, ϕ) space is shifted, but its size remains approximately the same,

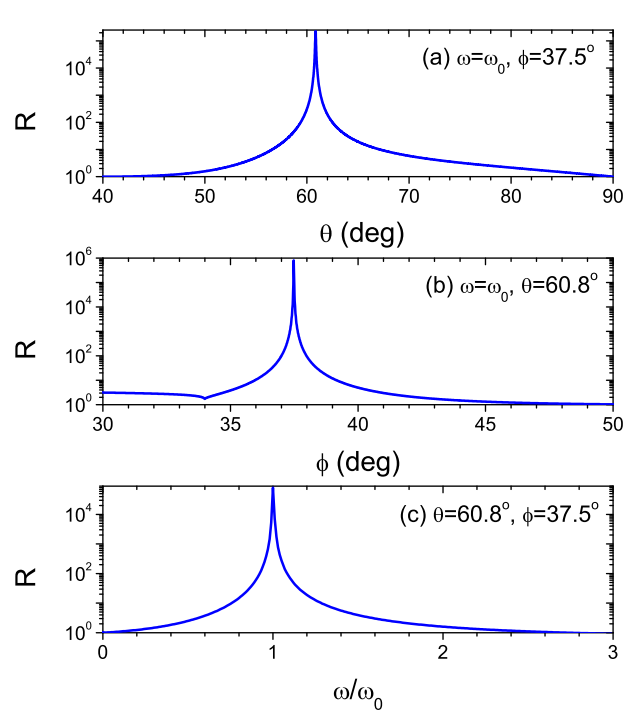


Figure 6. Reflectance R plotted (a) versus θ when $\omega = \omega_0$ and $\phi = 37.5^\circ$, (b) versus ϕ when $\omega = \omega_0$ and $\theta = 60.8^\circ$, and (c) versus ω/ω_0 when $\theta = 60.8^\circ$ and $\phi = 37.5^\circ$ for the configuration given by Eq. (52). The plasma β is zero.

as β increases. Therefore the finite temperature effect does not destroy the giant overreflection.

Giant overreflection also occurs for slow waves, which exist only in finite temperature plasmas. The parameter values that generate strong overreflection for slow waves are substantially different from those for fast waves. In Fig. 8, we have considered the configuration given by

$$\frac{U_x(z)}{v_{A1}} = \begin{cases} 7, & \text{if } z < 0 \\ 7(1 - \frac{z}{L}), & \text{if } 0 \leq z \leq L, \\ 0, & \text{if } z > L \end{cases}$$

$$\frac{v_A(z)}{v_{A1}} = \begin{cases} 4, & \text{if } z < 0 \\ 4 - 3\frac{z}{L}, & \text{if } 0 \leq z \leq L, \\ 1, & \text{if } z > L \end{cases} \quad (53)$$

and chosen $\beta = 0.1$ and $\omega = 0.2\omega_0$. We find that, though the maximum reflectance is only of the order of 10^3 , the region where R is larger than 10 is much wider than that corresponding to fast waves. This result suggests that even for values of β as small as 0.1, slow waves and slow resonances may play rather important roles in various processes in space plasmas. The elongated

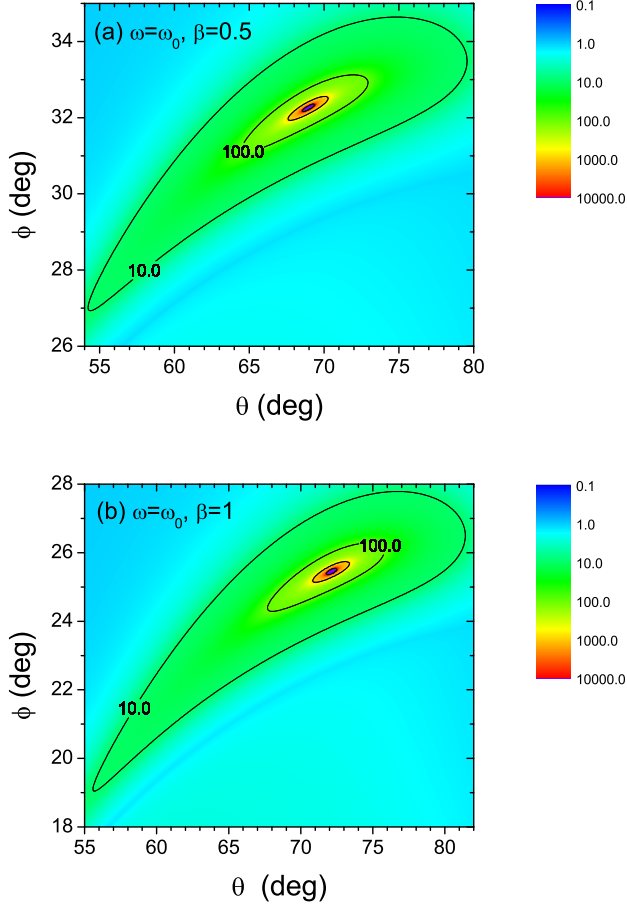


Figure 7. Logarithmic contour plots of R for fast waves of frequency $\omega = \omega_0$ versus θ and ϕ for the configuration given by Eq. (52), when (a) $\beta = 0.5$ and (b) $\beta = 1$.

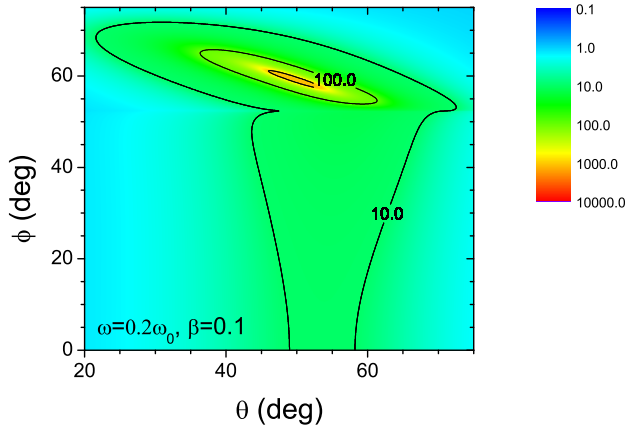


Figure 8. Logarithmic contour plot of R for slow waves of frequency $\omega = 0.2\omega_0$ versus θ and ϕ for the configuration given by Eq. (53), when $\beta = 0.1$.

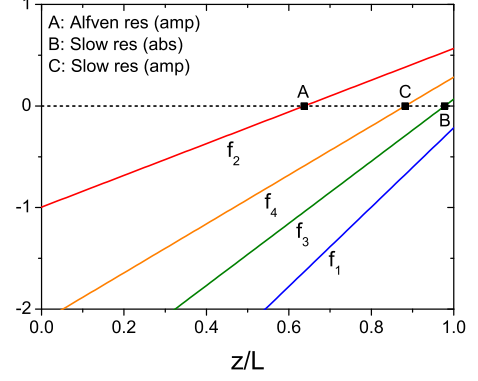


Figure 9. The functions f_1 , f_2 , f_3 , and f_4 defined by Eq. (34) for the configuration given by Eq. (53) plotted versus z/L when $\theta = 49.9^\circ$ and $\phi = 59.3^\circ$, which corresponds to the maximum value of R in Fig. 8. The resonant amplification due to the Alfvén resonance occurs at the position A ($z/L \approx 0.637$) and the resonant absorption and amplification due to the slow resonance occur at the positions B ($z/L \approx 0.978$) and C ($z/L \approx 0.882$) respectively.

region with $\phi \lesssim 52.3^\circ$ where $R > 10$ corresponds to the region where strong overreflection occurs due to negative energy waves in the transmitted region.

At finite temperatures, both Alfvén and slow resonances can occur simultaneously inside the inhomogeneous plasma. In Fig. 9, we plot the functions f_1 , f_2 , f_3 , and f_4 defined by Eq. (34) for the configuration given by Eq. (53) versus z/L when $\theta = 49.9^\circ$ and $\phi = 59.3^\circ$, which corresponds to the maximum of R in Fig. 8. The resonant amplification due to the Alfvén resonance occurs at the position A ($z/L \approx 0.637$) and the resonant absorption and amplification due to the slow resonance occur at the positions B ($z/L \approx 0.978$) and C ($z/L \approx 0.882$) respectively. We notice that two different types of resonances are responsible for the giant overreflection in this case.

Strong overreflection and amplification of magnetosonic waves are not limited to specific configurations and occur in a wide range of configurations for the flow velocity and the plasma density. In Fig. 10, we consider the configuration given by

$$\begin{aligned} \frac{U_x(z)}{v_{A1}} &= \begin{cases} 7, & \text{if } z < 0 \\ 7(1 - \frac{z}{L}), & \text{if } 0 \leq z \leq L, \\ 0, & \text{if } z > L \end{cases} \\ \frac{\rho_0(z)}{\rho_{01}} &= \begin{cases} 0.1, & \text{if } z < 0 \\ 0.9\frac{z}{L} + 0.1, & \text{if } 0 \leq z \leq L, \\ 1, & \text{if } z > L \end{cases} \end{aligned} \quad (54)$$

where the plasma density ρ_0 , instead of the Alfvén velocity v_A , varies linearly inside the inhomogeneous slab.

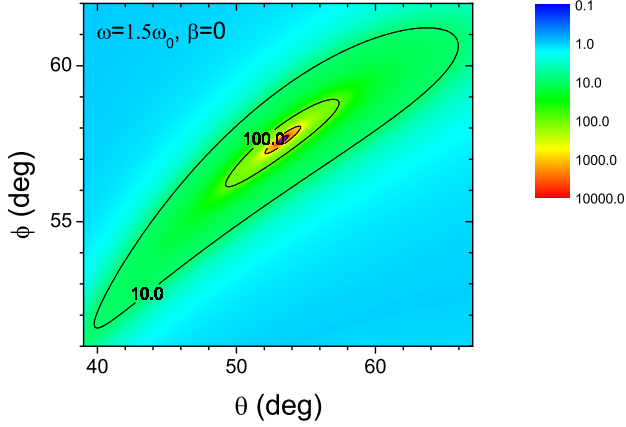


Figure 10. Logarithmic contour plot of R versus θ and ϕ for the configuration given by Eq. (54), when $\omega = 1.5\omega_0$ and $\beta = 0$.

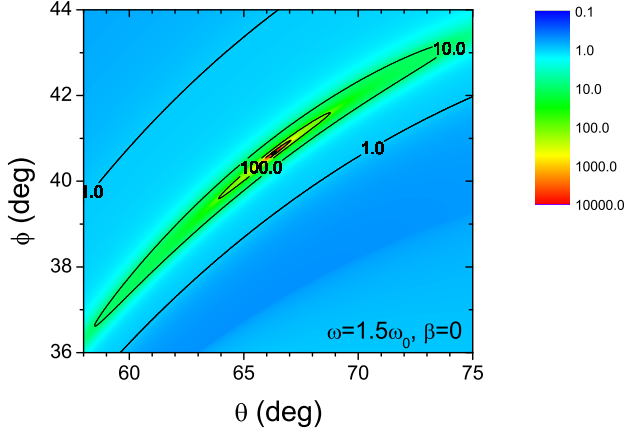


Figure 11. Logarithmic contour plot of R versus θ and ϕ for the configuration given by Eq. (55), when $\omega = 1.5\omega_0$ and $\beta = 0$.

We find that giant overreflection occurs in a wide range of θ and ϕ in this case too.

In Fig. 11, we consider the configuration given by

$$\frac{U_x(z)}{v_{A1}} = \begin{cases} 2.5, & \text{if } z < 0 \\ 2.5 \left(1 - \frac{z}{L}\right), & \text{if } 0 \leq z \leq L, \\ 0, & \text{if } z > L \end{cases}$$

$$\frac{v_A(z)}{v_{A1}} = \begin{cases} 0.9, & \text{if } z < 0 \\ 0.9 + 0.1 \frac{z}{L}, & \text{if } 0 \leq z \leq L, \\ 1, & \text{if } z > L \end{cases}, \quad (55)$$

where the Alfvén velocity decreases (therefore, the plasma density increases) as z decreases from L to 0 , in contrast to the cases considered so far. Since the wave is incident from the region where $z > L$, it propagates

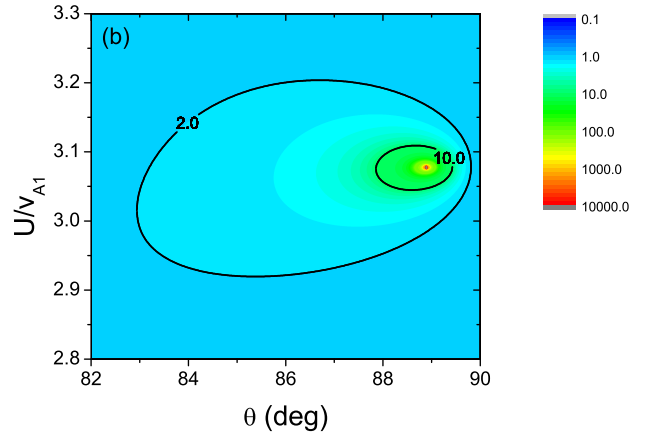
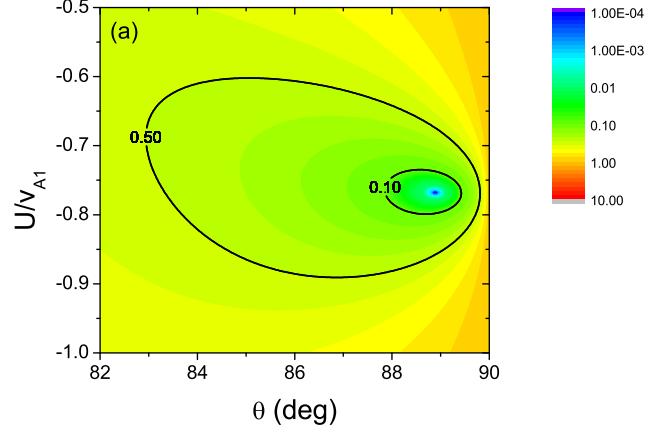


Figure 12. Logarithmic contour plots of R versus θ and U/v_{A1} for the configuration given by Eq. (56), when $\phi = 30^\circ$, $\omega/\omega_0 = \pi$, and $\beta = 0$. The regions where R is (a) smaller than 0.5 and (b) larger than 2 are explicitly displayed.

from the region of lower density into that of higher density and gets reflected. In this case, we find that the region where total reflection occurs and the transmission vanishes is narrow. Since strong overreflection occurs mostly when total reflection does, the parameter region where strong overreflection occurs is rather narrow in the present configuration, though it is still in a readily observable range of the (θ, ϕ) space.

We have also performed calculations for much larger values of the damping parameter up to $\eta = 1$. Up to $\eta \approx 0.1$, we have verified that there is no noticeable change in the position and the size of the region where R is strongly amplified in the (θ, ϕ) space. For $\eta > 0.1$, the position of this region is shifted, but its size remains substantially large. We conclude that the phenomenon of giant overreflection persists even in the presence of realistic damping.

6. MECHANISM OF GIANT OVERREFLECTION

From the results presented so far, we conclude that giant overreflection and amplification of incident magnetosonic waves is a generic and robust phenomenon in inhomogeneous plasmas with nonuniform shear flows. We now attempt to explain the origin of this phenomenon. To provide a simpler and more transparent explanation, it is beneficial to consider a configuration where the flow velocity is uniform in the half space, such as given by

$$U_x(z) = \begin{cases} U, & \text{if } z \leq L \\ 0, & \text{if } z > L \end{cases},$$

$$\frac{\rho_0(z)}{\rho_{01}} = \begin{cases} 0.1, & \text{if } z < 0 \\ 0.9\frac{z}{L} + 0.1, & \text{if } 0 \leq z \leq L \\ 1, & \text{if } z > L \end{cases}. \quad (56)$$

We fix $\beta = 0$, $\omega/\omega_0 = \pi$, and $\phi = 30^\circ$ and calculate R and T as a function of U and θ . In Fig. 12, we show the logarithmic contour plots in the two regions where R is smaller than 0.5 and larger than 2. We observe that there is a perfect symmetry between the shapes of these regions. This symmetry can be understood easily from the complex form of ϵ given in Eq. (43). There always exist a pair of U values, U_a and U_b , for any configuration of ρ_0 and for any values of θ and ϕ , such that the corresponding values of ϵ are the complex conjugates of each other, that is, $\epsilon^*(U_a) = \epsilon(U_b)$. From Eq. (43), we obtain

$$\frac{U_a}{v_{A1}} + \frac{U_b}{v_{A1}} = \frac{2}{\sin \theta \cos \phi}, \quad (57)$$

which explains the symmetry between Figs. 12(a) and 12(b) very well.

The wave scattering coefficients for the medium with the scattering potential ϵ are closely related to those for the medium with the scattering potential ϵ^* . These relationships can be derived from scattering theory. For a given medium, one needs to consider the reflection and transmission coefficients, r_R and t_R (r_L and t_L) for the waves incident from the right (left). We only need the relationship

$$[r_R(\epsilon^*)]^* = \frac{r_L(\epsilon)}{r_R(\epsilon)r_L(\epsilon) - t_R(\epsilon)t_L(\epsilon)}, \quad (58)$$

which has been derived in Rivero & Ge (2019). For the consideration of the giant overreflection, we are mainly interested in the case where the wave is evanescent in the transmitted region and the transmission coefficients t_R and t_L vanish. Then we obtain a very simple relationship between the reflectances for ϵ and ϵ^* of the form

$$R(\epsilon^*) = \frac{1}{R(\epsilon)}. \quad (59)$$

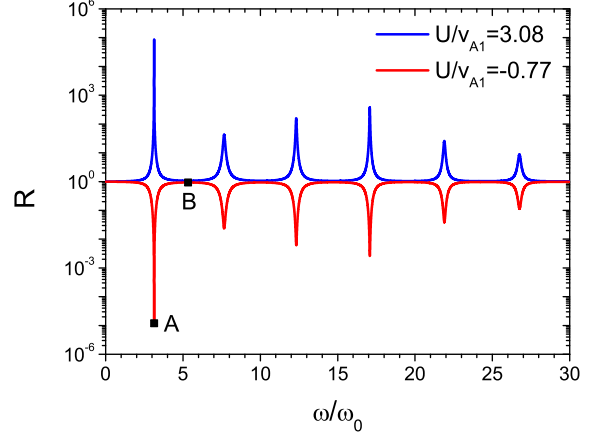


Figure 13. Reflectance versus normalized frequency ω/ω_0 for the configuration given by Eq. (56), when $\theta = 88.89^\circ$, $\phi = 30^\circ$, $\beta = 0$, and $U/v_{A1} = 3.08, -0.77$. The two reflectances are precisely the reciprocal of each other. The points A and B correspond to $\omega/\omega_0 = 3.13$ and 5.32 respectively.

We have verified that this relationship is strictly satisfied for U_a and U_b satisfying Eq. (57), as can be checked in Fig. 12.

In the configuration given by Eq. (56) and when $\phi = 30^\circ$ and $\beta = 0$, the reflectance becomes extremely small and the plasma behaves as a near-perfect absorber when $U/v_{A1} = -0.77$ and $\theta = 88.89^\circ$. For this case, the conjugate value of U obtained from Eq. (57) is $U/v_{A1} = 3.08$. In Fig. 13, we show how the reflectance varies as a function of the frequency for these two conjugate cases. We find that the two reflectances are precisely the reciprocal of each other in excellent agreement with Eq. (59). It is intriguing that *the near-perfect absorption and the giant overreflection arise as a pair of conjugate phenomena*. Many sharp peaks and dips appear in a regular pattern resembling a Fabry-Perot resonator in Fig. 13, with approximately equal intervals between them. This suggests clearly that some kind of resonance phenomenon associated with a cavity is taking place.

From the wave equation, Eq. (40), we notice that the quantity

$$\kappa(z) \equiv \sin^2 \theta \sin^2 \phi - \epsilon(z) \quad (60)$$

can be considered as the negative square of the z component of the wave vector. The wave becomes evanescent where κ is positive. In Fig. 14, we plot κ versus z/L when $\theta = 88.89^\circ$, $\phi = 30^\circ$, and $U/v_{A1} = 3.08$ (or -0.77). We note that κ is the same for both $U/v_{A1} = 3.08$ and -0.77 . The wave is evanescent in the region $z < z_{co}$ ($\approx 0.29L$). The position of the Alfvén resonance z_A ($\approx 0.19L$) is located inside the evanescent region. We point out that κ plays the role of a scattering po-

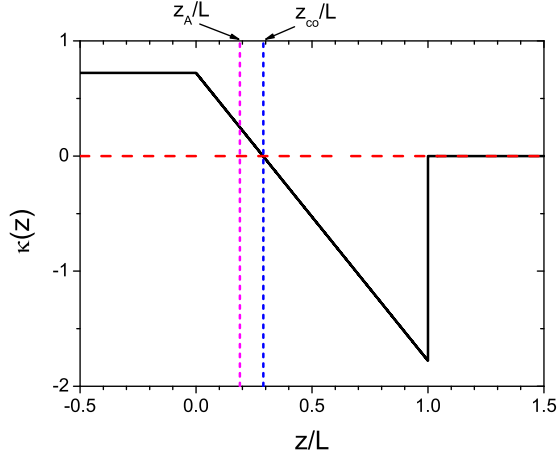


Figure 14. The function $\kappa(z)$ [$\equiv \sin^2 \theta \sin^2 \phi - \epsilon(z)$], where $\epsilon(z)$ is given by Eq. (41), plotted versus z/L for the configuration given by Eq. (56), when $\theta = 88.89^\circ$, $\phi = 30^\circ$, and $U/v_{A1} = 3.08$ (or -0.77). The wave becomes evanescent in the region $z < z_{co}$ ($\approx 0.29L$) where κ is positive. z_A ($\approx 0.19L$) denotes the position of the Alfvén resonance.

tential and an effective cavity is formed in the region $0.29 < z/L < 1$. Note that this is an *open cavity* since the wave can propagate through one end at $z = L$. In the present case, however, a series of semi-bound states are well-formed, since the absolute value of κ is very small in $z > L$. The formation of semi-bound states is the cause of both extremely small reflectance and perfect absorption for $U/v_{A1} = -0.77$ and extremely large reflectance and amplification for $U/v_{A1} = 3.08$.

In Fig. 15, we plot the spatial distributions of the intensity of the x component of the magnetic field, $|B_x|^2$, obtained by solving Eq. (50), when $\theta = 88.89^\circ$, $\phi = 30^\circ$, $U/v_{A1} = -0.77$, and $\omega/\omega_0 = 3.13$ and 5.32 , which correspond to the points A and B denoted in Fig. 13 respectively. When ω/ω_0 is 3.13 , corresponding to the minimum reflectance close to zero, the field profile shows an antinode at $z = L$, whereas, when ω/ω_0 is 5.32 , corresponding to the reflectance close to unity, the field profile shows a node at $z = L$. This result is fully consistent with the formation of a semi-bound state in an open cavity.

7. DISCUSSION

Let us first estimate the possibility of observing the phenomena predicted in this paper in the terrestrial magnetosphere. In the configuration given by Eq. (52), the range of the variation and the maximum value of the flow velocity are 2.5 and $5/3$ times those of the Alfvén velocity respectively and an incident wave propagates from a higher density region to a lower density region. The flow speed is slightly super-Alfvénic in

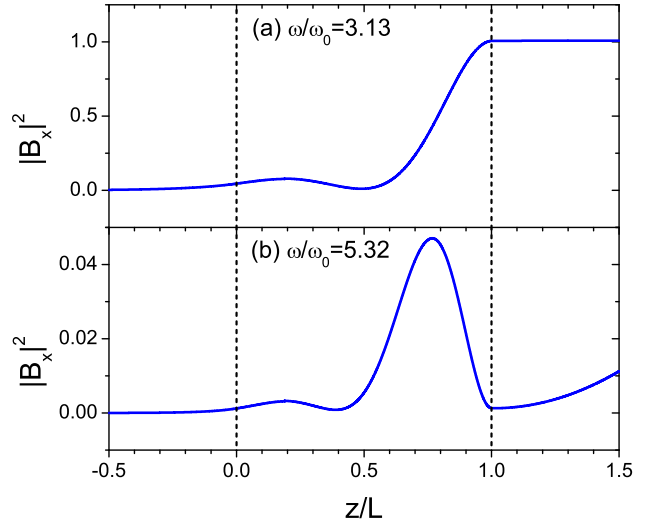


Figure 15. Spatial distributions of the intensity of the x component of the magnetic field, $|B_x|^2$, for the configuration given by Eq. (56), when $\theta = 88.89^\circ$, $\phi = 30^\circ$, $\beta = 0$, $U/v_{A1} = -0.77$, and (a) $\omega/\omega_0 = 3.13$ and (b) $\omega/\omega_0 = 5.32$, which correspond to the points A and B in Fig. 13 respectively. The wave is assumed to be incident from the right side. The vertical dashed lines denote the position of the inhomogeneous slab.

$0 < z/L < 2/3$ and sub-Alfvénic in $2/3 < z/L < 1$. From the numerical results, strong overreflection with the reflectance greater than 10 is found to arise in a broad range of the parameter values when the wave frequency f is roughly in the range of

$$0.5f_0 \lesssim f \lesssim 1.5f_0, \quad (61)$$

where the unit frequency f_0 is defined by

$$f_0 = \frac{\omega_0}{2\pi} = \frac{v_{A1}}{2\pi L}. \quad (62)$$

As an example, we choose L to be the thickness of the dawnside magnetopause in the Earth's magnetosphere, which has been reported to be about 1500 km (Haaland et al. 2019). If we also assume, reasonably, that the Alfvén velocity in the incident region is about 200 km/s, then f_0 is about 21 mHz and the frequency range of strong overreflection is between 10 and 32 mHz, which is well within the region of Pc 3–4 magnetic pulsations. Strong overreflection occurs also in the case where an incident wave propagates from a lower density region to a higher density region and for many other different configurations. This consideration appears to support the proposition that strong overreflection takes place widely in the magnetopause region and may contribute

to the excitation and enhancement of ULF magnetic pulsations. We also speculate that this phenomenon could be an energy source of giant pulsations (Pg) with large field amplitudes (Wright et al. 2001).

Similar estimates can be made for other astrophysical plasmas including the solar atmosphere. In finite β plasmas, both slow magnetosonic waves and slow resonances can contribute substantially to strong overreflection. In the configuration given by Eq. (53) and considered in Fig. 8, the range of the variation and the maximum value of the flow velocity are $7/3$ and $7/4$ times those of the Alfvén velocity respectively and an incident wave propagates from a higher density region to a lower density region. The flow speed is super-Alfvénic in $0 < z/L < 0.75$ and sub-Alfvénic in $0.75 < z/L < 1$. From Fig. 8, we observe that giant overreflection occurs for a very wide range of the incident angles when slow magnetosonic waves are incident. The plasma β and the frequency used in the calculation are $\beta = 0.1$, which is a reasonable value for the lower part of the transition layer between the solar chromosphere and the corona, and $f = 0.2f_0$. We notice that giant overreflection occurs at a considerably lower frequency range for slow waves than for fast waves. If, for instance, we assume that L is 500 km and v_{A1} is 100 km/s, then f_0 is about 32 mHz. In that case, giant overreflection for slow waves is expected when the frequency is about 6 mHz and the oscillation period is about 160 seconds.

Finally, we speculate that giant overreflection may provide an alternative route for plasma heating. Overreflection causes the flow kinetic energy to be converted into the wave energy. The amplified MHD waves will propagate through various regions of the plasma and may induce resonant absorption or another overreflection. Ultimately, the energy of the wave will be converted into heat by some dissipative mechanism. This can be a multi-step route of plasma heating.

8. CONCLUSION

In this paper, we have investigated the mode conversion and resonant overreflection of MHD waves in an in-

homogeneous plasma with a nonuniform mass flow theoretically, using the IIM. We have found that, especially when the parameters are such that the incident waves are totally reflected, giant overreflection where the reflectance is much larger than 10 arises in a universal manner. It occurs in a fairly broad range of the incident angles, the frequency, and the plasma β and occurs for many different types of the density and flow velocity profiles. We have also found that in finite β plasmas, slow magnetosonic waves and slow resonances cause strong overreflection in a broader range of parameters than fast magnetosonic waves. This result suggests that slow waves may play important roles in various processes in space plasmas.

In the present work, we have been mainly concerned with the calculation of the reflectance and the transmittance and presented only limited results of the spatial field distributions. However, it is straightforward to calculate all the components of various fields using the IIM, which can provide valuable informations about polarization, compression, vorticity, and other characteristics (Goossens et al. 2020, 2021). Our method also allows to consider the more general case where the magnetic field as well as the plasma density and the flow velocity is inhomogeneous. With such a generalization, one can study interesting subjects such as the magnetic reconnection region and the coronal plume structure (Provornikova et al. 2018; Andries et al. 2000). Future work in these directions will be of great interest.

- 1 This research was supported through a National
- 2 Research Foundation of Korea Grant (NRF-
- 3 2022R1F1A1074463) funded by the Korean Govern-
- 4 ment. It was also supported by the Basic Science
- 5 Research Program funded by the Ministry of Education
- 6 (2021R1A6A1A10044950) and by the Global Frontier
- 7 Program (2014M3A6B3063708).

REFERENCES

- Andries, J., Tirry, W. J., & Goossens, M. 2000, *ApJ*, 531, 561
- Bellman, R., & Wing, G. M. 1976, *An Introduction to Invariant Imbedding* (New York: Wiley)
- Čadež, V. M., Csík, Á., Erdélyi, R., & Goossens, M. 1997, *A&A*, 326, 1241
- Cairns, R. A. 1979, *J. Fluid Mech.*, 92, 1
- Chen, L., & Hasegawa, A. 1974a, *Phys. Fluids*, 17, 1399
- Chen, L., & Hasegawa, A. 1974b, *J. Geophys. Res.*, 79, 1024
- Csík, Á. T., Čadež, V. M., & Goossens, M. 1998, *A&A*, 339, 215
- Csík, Á. T., Čadež, V. M., & Goossens, M. 2000, *A&A*, 358, 1090
- Forslund, D. W., Kindel, J. M., Lee, K., Lindman, E. L., & Morse, R. L. 1975, *PhRvA*, 11, 679
- Golberg, M. A. 1975, *Appl. Math. Comput.*, 1, 1

- Goossens, M., Arregui, I., Soler, R., & Van Doorselaere, T. 2020, *A&A*, 641, A106
- Goossens, M., Chen, S.-X., Geeraerts, M., Li, B., & Van Doorselaere, T. 2021, *A&A*, 646, A86
- Haaland, S., Runov, A., Artemyev, A., & Angelopoulos, V. 2019, *J. Geophys. Res. Space Phys.*, 124, 3421
- Hinkel-Lipsker, D. E., Fried, B. D., & Morales, G. J. 1992, *Phys. Fluids B*, 4, 559
- Joarder, P. S., Nakariakov, V. M., & Roberts, B. 1997, *SoPh*, 176, 285
- Keiling, A., Lee, D.-H., & Nakariakov, V. 2016, *Low-Frequency Waves in Space Plasmas* (Washington, D.C., Hoboken, NJ: American Geophysical Union, Wiley)
- Kim, K., & Lee, D.-H. 2005, *Phys. Plasmas*, 12, 062101
- Kim, K., & Lee, D.-H. 2006, *Phys. Plasmas*, 13, 042103
- Kim, E.-H., Cairns, I. H., & Robinson, P. A. 2007, *PhRvL*, 99, 015003
- Kim, S., & Kim, K. 2016a, *J. Opt.*, 18, 065605
- Kim, S., & Kim, K. 2016b, *Opt. Express*, 24, 1794
- Klyatskin, V. I. 2005, *Stochastic Equations through the Eye of the Physicist* (Amsterdam: Elsevier)
- Lee, D.-H., Hudson, M. K., Kim, K., Lysak, R. L., & Song, Y. 2002, *J. Geophys. Res.*, 107, 1307
- Lee, D.-H., Johnson, J. R., Kim, K., & Kim, K.-S. 2008, *J. Geophys. Res.*, 113, A11212
- Leonovich, A. S., & Kozlov, D. A. 2013, *Earth Planets Space*, 65, 369
- Lysak, R. L. 2022, *Front. Astron. Space Sci.*, 9, 913554
- Mann, I. R., Wright, A. N., Mills, K. J., & Nakariakov, V. M. 1999, *J. Geophys. Res.*, 104, 333
- Mazur, V. A., & Chuiko, D. A. 2013, *Plasma Phys. Rep.*, 39, 959
- McDougall, A. M. D. & Hood, A. W. 2007, *SoPh*, 246, 259
- McKenzie, J. F. 1970, *Planet. Space Sci.*, 18, 1
- Mjølhus, E. 1990, *Radio Sci.*, 25, 1321
- Nakariakov, V. M., Pilipenko, V., Heilig, B., et al. 2016, *SSRv*, 200, 75
- Nakariakov, V. M. & Kolotkov, D. Y. 2020, *ARA&A*, 58, 441, doi:10.1146/annurev-astro-032320-042940
- Ostrovskii, L. A., Rybak, S. A., & Tsimring, L. Sh. 1986, *Sov. Phys. Usp.*, 29, 1040
- Provornikova, E., Laming, J. M., & Lukin, V. S. 2018, *ApJ*, 860, 138
- Rivero, J. D. H., & Ge, L. 2019, *PhRvA*, 100, 023819
- Roberts, B. 2019, *MHD Waves in the Solar Atmosphere* (Cambridge: Cambridge University Press)
- Swanson, D. G. 1998, *Theory of Mode Conversion and Tunneling in Inhomogeneous Plasmas* (New York: Wiley)
- Southwood, D. J. 1974, *Planet. Space Sci.*, 22, 483
- Van Doorselaere, T., Srivastava, A. K., Antolin, P., et al. 2020, *SSRv*, 216, 140. doi:10.1007/s11214-020-00770-y
- Walker, A. D. M. 1998, *J. Atmos. Sol. Terr. Phys.*, 60, 1279
- Walker, A. D. M. 2000, *J. Atmos. Sol. Terr. Phys.*, 62, 799
- Walker, A. D. M. 2005, *Magnetohydrodynamic Waves in Geospace* (Bristol: Institute of Physics Publishing)
- Wright, D. M., Yeoman, T. K., Rae, I. J., et al. 2001, *J. Geophys. Res.*, 106, 10837
- Yu, D. J. & Nakariakov, V. M. 2020, *ApJ*, 896, 21, doi:10.3847/1538-4357/ab8d3c